Prediction of induced soil vibration during pile vibrodriving using Dynamic Mode Decomposition (DMD)

Journal of Physics: Conference Series **2909** (2024) 012002 doi:10.1088/1742-6596/2909/1/012002

Prediction of induced soil vibration during pile vibrodriving using Dynamic Mode Decomposition (DMD)

Francisco Williams-Riquer, Alexander Chmelnizkij, Diaa Alkateeb and Jürgen Grabe

Hamburg University of Technology, Hamburg, Germany

E-mail: francisco.williams@tuhh.de, alexander.chmelnizkij@tuhh.de, diaa.alkateeb@tuhh.de, grabe@tuhh.de

Abstract.

This study investigates using the Dynamic Mode Decomposition (DMD) algorithm to perform approximations and time-ahead prediction of soil vibrations during the vibrodriving process. Geotechnical applications face challenges in modeling and predicting soil vibrations due to the soil's heterogeneous nature. This study addresses this issue using a purely data-driven approach. Geophone data collected during pile installation using a vibrodriver were used to demonstrate the feasibility of the DMD algorithm. The research reveals that both the standard DMD and augmented DMD, which incorporate delay coordinates, can achieve accurate predictions, with the augmented DMD producing more accurate time-ahead predictions of the vibrations. The results emphasize the potential practical utility of data-driven methods for vibration prediction in geotechnical applications.

1. Introduction

Vibrodriving is a technique used for pile installation. It involves coupling an unbalanced vibrator to the pile, which generates a harmonic excitation force. This force can induce local compaction, loosening, and soil displacement around the pile. Compared to the impact-driven technique, vibrodriving requires smaller loads and allows for a faster penetration rate while minimizing damage to the pile [1]. The primary goal of pile installation is to reach the desired depth while minimizing adverse environmental effects such as vibration and noise that could affect structures and people [2]. Contractors typically select a vibrator based on their experience. The feed parameters such as frequency, amplitude, and surcharge force are chosen empirically [3, 2]. The foundation phase is the most demanding regarding construction projects' labor costs and time requirements [4]. Therefore, there is a growing interest in automating the pile installation process due to its market potential [5].

1.1. Ground vibration modelling and prediction

The accurate monitoring and prediction of ground vibrations during pile vibrodriving is crucial due to their potential to disturb residents and occupants of nearby buildings [6, 3, 7]. Notably, even vibrations as low as 0.1 mm/s in the 1 to 80 Hz frequency range can be perceptible to the human body [2]. While previous literature has addressed this issue, a conclusive methodology

is yet to be established. Existing analytical solutions are limited, focusing solely on foundation elements and neglecting factors such as inhomogeneities and the influence of multiple soil layers [8]. Based on the half-space assumption, these studies overlook the impact of local geological conditions on ground motion amplitudes [9]. Some studies have proposed regression models to fit data sets visually, but no satisfactory method for estimating vibrations has been identified [10]. The consensus from these investigations is that preliminary measurements, utilizing tools like geophones, offer the most satisfactory means of estimating surface vibrations transmitted to the surroundings due to the significant variations in conditions observed from site to site [10, 6].

An alternative method for modeling and predicting ground vibrations during pile installation involves utilizing numerical models, i.e., Finite Element Method (FEM). Various authors have tackled this challenge using diverse techniques and constitutive models, ranging from the Mohr-Coulomb model [11] to more intricate models like Hypoplasticity, which specifically addresses the nonlinear and anelastic behavior of sand [12]. However, the validation of FEM simulations typically necessitates comparison with field measurements to ensure their accuracy [12, 11, 13]. Once validated, these simulations exhibit favorable agreement with test data, including the simulation of wave propagation [12]. The primary objective of these simulations is usually parameter variation, providing practicing engineers with an initial estimate of additional loads on existing structures [13]. This investigative process contributes to the validation and enhancement of industry standards [14]. Nevertheless, it is crucial to acknowledge that these simulations operate under certain assumptions that can sometimes result in significant discrepancies with reality [11]. Despite their advantages, FEM simulations come with drawbacks. They demand substantial computational power and cannot be executed in real-time as a tool for selecting feed parameters in the field. Furthermore, conducting such simulations requires a comprehensive understanding of the in-situ soil conditions, necessitating laboratory testing for soil characterization.

1.2. Motivation

The goals of pile installation present a fundamental contradiction: the need for fast pile penetration clashes with the imperative to limit transmitted ground vibrations [15]. Consequently, any automation strategy must grapple with these conflicting objectives. Despite the issue's significance, currently used control systems offer limited opportunities for optimizing the overall process. Recent control strategies primarily optimize power consumption and achieve gearless mass synchronization. These strategies use model-based, usually linear, control leveraging the well-defined equations describing the hardware mechanics [16, 17, 18]. However, given the lack of reliable and simple mathematical models, they have yet to incorporate information regarding the vibrations transmitted to the soil. Alternatively, some strategies involve deriving fuzzy logic controllers based on empirical relations and field measurements [15]. Therefore, a notable gap in research still exists concerning integrating control strategies capable of successfully conducting online predictions of vibrations, considering local and varying geological conditions, and adapting the feed parameters in real time. For the reasons mentioned, it becomes evident that predictions based on analytical solutions relying on the half-space and Finite Element Method (FEM) simulations fall short for this specific task.

In this work, we present the first steps to bring vibration prediction to a framework that can eventually be integrated into a control system to automate the vibrodriving process optimally. We take a distinctive approach to vibration prediction by employing an equation-free, purely data-driven method called Dynamic Mode Decomposition (DMD) and, thus, bypassing the complications of FEM models and the oversimplification of analytical models while considering local geological conditions during the process. Originating from the fluid dynamics community and first introduced in [19], DMD aims to accurately decompose a complex system into spatiotemporal coherent structures. These structures can then be utilized for short-term future

predictions and control [20].

This manuscript is arranged as follows: Section 2 introduces the DMD framework and the use of delay coordinates. Section 3 summarises the measurement campaign, where piles were installed using vibrodrivers and geophone data was collected. Section 4 presents a systematic study of the DMD capabilities to perform time-ahead prediction of the vibrations using the accumulated data in the measurement campaign and its efficiency. Finally, Section 5 presents an outline of the future work required and concludes.

2. Dynamic Mode Decomposition

This section introduces the Dynamic Mode Decomposition (DMD) algorithm, including its mathematical framework. For a thorough inquiry, readers are recommended to refer to the extensive works of [20] and [21]. The DMD method facilitates a spatiotemporal breakdown of data, revealing dynamic modes derived from snapshots or measurements taken over time from a given system. Consider a general dynamical system described by ordinary differential equations, represented as

$$\frac{d\mathbf{x}}{dt} = f(\mathbf{x}, t, \mu), \tag{1}$$

where $\mathbf{x}(t) \in \mathbb{R}^n$ denotes the n states of the system at time t, μ encompasses system parameters, and $f(\cdot)$ characterizes the system's dynamics.

The discrete-time representation of Eq. (1) is given by

$$\mathbf{x}_{k+1} = \mathbf{F}(\mathbf{x}_k), \tag{2}$$

where $\mathbf{x}_k = \mathbf{x}(k\Delta t)$ represents the discrete-state vector for $k = 1, 2, ..., m$, Δt is the time-sample period, m the total number of measurements and $\mathbf{F}$ the corresponding mapping from $\mathbb{R}^n \mapsto \mathbb{R}^n$. The vector $\mathbf{x}_k$ results from the discretization of a complex system or direct sensor measurements. DMD can utilize data measurements to approximate dynamics and predict future states. It introduces a linearization at different time instants as

$$\frac{d\mathbf{x}}{dt} = \mathcal{A}\mathbf{x}, \tag{3}$$

with the initial condition $\mathbf{x}(0)$ and the solution:

$$\mathbf{x}(t) = \sum_{k=1}^{n} \phi_k \exp(\omega_k t) b_k = \mathbf{\Phi} \exp(\mathbf{\Omega} t)\mathbf{b}. \tag{4}$$

From Eq. 4, Ω is a diagonal matrix containing the eigenvalues ω_k of $\mathcal{A}$, Φ is the eigenvector matrix with eigenvectors ϕ_k of $\mathcal{A}$, and $\mathbf{b}$ contains the coefficients resulting from the initial conditions $\mathbf{x}(0)$ in the eigenvector basis. Analogously, a discrete-time system sampled every Δt is described as

$$\mathbf{x}_{k+1} = \mathbf{A}\mathbf{x}_k, \tag{5}$$

where $\mathbf{A} = \exp(\mathcal{A}\Delta t)$, and the discrete-time solution is given by

$$\mathbf{x}_{k+1} = \sum_{j=1}^{r} \phi_j \lambda_j^k b_j = \mathbf{\Phi}\mathbf{\Lambda}^k\mathbf{b}, \tag{6}$$

where $\mathbf{\Lambda}^k$ is a diagonal matrix containing the discrete-time eigenvalues of $\mathbf{A}$. The DMD algorithm produces a low-rank approximation of matrix $\mathbf{A}$ that optimally fits the measured

trajectory $\mathbf{x}_k$ for $k = 1, 2, ..., m$ in a least-square sense. This optimization minimizes Eq. 7 across all points for $k = 1, 2, ..., m-1$.

$$\|\mathbf{x}_{k+1} - \mathbf{A}\mathbf{x}_k\|_2 \tag{7}$$

The optimal approximation holds only over the sampling window where $\mathbf{A}$ is constructed and can be employed for making future state predictions.

To minimize Eq. 7 across all snapshots from $k = 1, 2, ..., m$, it is possible to arrange the m snapshots into two large data matrices:

$$\mathbf{X}_1 = \begin{bmatrix} | & | & & | \\ \mathbf{x}_1 & \mathbf{x}_2 & \cdots & \mathbf{x}_{m-1} \\ | & | & & | \end{bmatrix}, \tag{8a}$$

$$\mathbf{X}_2 = \begin{bmatrix} | & | & & | \\ \mathbf{x}_2 & \mathbf{x}_3 & \cdots & \mathbf{x}_{m} \\ | & | & & | \end{bmatrix}, \tag{8b}$$

where $\mathbf{X}_1, \mathbf{X}_2 \in \mathbb{R}^{n \times (m-1)}$. The local linear approximation in Eq. 5 is then written as

$$\mathbf{X}_2 \approx \mathbf{A}\mathbf{X}_1 \tag{9}$$

Therefore, the best-fit $\mathbf{A}$ matrix is given by

$$\mathbf{A} = \mathbf{X}_1\mathbf{X}_2^{+} \tag{10}$$

where $\mathbf{X}_2^{+}$ is the Moore-Penrose pseudoinverse. The DMD modes, also called dynamic modes, are the eigenvectors of $\mathbf{A}$, and each DMD mode corresponds to a particular eigenvalue of $\mathbf{A}$.

2.1. Delay coordinates and shift-stacking

For applications where state measurements are inherently low-dimensional, introducing delay coordinates becomes crucial to augment the matrix rank effectively [20]. We can then construct an augmented vector by incorporating s time-shifted state vectors $\mathbf{x}$ from future or past instances. This augmentation is reflected in creating the matrices:

$$\mathbf{X}_{1\,\mathrm{aug}} = \begin{bmatrix} \mathbf{x}_1 & \mathbf{x}_2 & \cdots & \mathbf{x}_{m-s} \\ \mathbf{x}_2 & \mathbf{x}_3 & \cdots & \mathbf{x}_{m-s+1} \\ \vdots & \vdots & \ddots & \vdots \\ \mathbf{x}_s & \mathbf{x}_{s+1} & \cdots & \mathbf{x}_{m-1} \end{bmatrix}, \tag{11a}$$

$$\mathbf{X}_{2\,\mathrm{aug}} = \begin{bmatrix} \mathbf{x}_2 & \mathbf{x}_3 & \cdots & \mathbf{x}_{m-s+1} \\ \mathbf{x}_3 & \mathbf{x}_4 & \cdots & \mathbf{x}_{m-s+2} \\ \vdots & \vdots & \ddots & \vdots \\ \mathbf{x}_{s+1} & \mathbf{x}_{s+2} & \cdots & \mathbf{x}_{m} \end{bmatrix}, \tag{11b}$$

with $\mathbf{X}_{1\,\mathrm{aug}}$, $\mathbf{X}_{2\,\mathrm{aug}} \in \mathbb{R}^{(s \times n) \times (m-s)}$. The parameter s can be systematically increased to improve the numerical rank. Subsequently, the DMD analysis is performed using the augmented matrices in the same manner as mentioned before. However, we retain only the first n rows of a Φ_{aug}.

2.2. DMD Algorithm

In practical scenarios where $n \gg 1$, direct analysis of the matrix $\mathbf{A}$ becomes impractical. Therefore, the DMD employs an economy Singular Value Decomposition (SVD) to overcome this. For a detailed exploration of the economy SVD, readers are encouraged to refer to works by [22] and [23].

This first step involves the consideration of the r truncation of the approximation to the matrix $\mathbf{X}_1$ using the economy SVD as in Eq. 12. This truncation is done after observing the contribution of the singular values and assuming a threshold that preserves enough information about the dynamical system.

$$\mathbf{X}_1 \approx \mathbf{U}\mathbf{\Sigma}\mathbf{V}^* \tag{12}$$

From Eq. 12: $\mathbf{U} \in \mathbb{C}^{n\times r}$, $\mathbf{\Sigma} \in \mathbb{C}^{r\times r}$, $\mathbf{V} \in \mathbb{C}^{m\times r}$, and * denotes the conjugate transpose. The $r \times r$ projection of matrix $\mathbf{A}$ is then calculated as:

$$\widetilde{\mathbf{A}} = \mathbf{U}^*\mathbf{A}\mathbf{U} = \mathbf{U}^*\mathbf{X}_2\mathbf{V}\mathbf{\Sigma}^{-1} \tag{13}$$

Utilizing $\widetilde{\mathbf{A}}$, a low-dimensional linear model of the dynamical system is defined as

$$\widetilde{\mathbf{x}}_{k+1} = \widetilde{\mathbf{A}}\widetilde{\mathbf{x}}_k, \tag{14}$$

where $\mathbf{x}_k = \mathbf{U}\widetilde{\mathbf{x}}_k$. The eigendecomposition of $\widetilde{\mathbf{A}}$ is then computed as

$$\widetilde{\mathbf{A}}\mathbf{W} = \mathbf{W}\mathbf{\Lambda}, \tag{15}$$

where the columns of $\mathbf{W}$ represent eigenvectors of $\widetilde{\mathbf{A}}$, and $\mathbf{\Lambda}$ is a diagonal matrix containing corresponding eigenvalues λ_k. Finally, reconstructing the eigendecomposition of $\mathbf{A}$ is possible, acknowledging that the eigenvalues of $\mathbf{A}$ match those of $\widetilde{\mathbf{A}}$. The eigenvectors (DMD modes) are given by the columns of $\mathbf{\Phi}$ as in Eq. 16.

$$\mathbf{\Phi} = \mathbf{X}_2\mathbf{V}\mathbf{\Sigma}^{-1}\mathbf{W} \tag{16}$$

This allows the construction of a prediction considering the coefficients b_k, the matrix $\mathbf{\Phi}$ with DMD modes ϕ_k, and a diagonal matrix $\mathbf{\Omega}$ with eigenvalues $\omega_k = \ln \lambda_k / \Delta t$, as defined in Eq. 4.

3. Measurement campaign

To test the performance of DMD in the time-ahead prediction of soil vibrations during pile installation, we used geophone data collected from installing three sheet piles (HP320) in Niederfinow, Germany [24]. The piles were installed to a depth of 18.3 m through a process that combined vibratory and impact driving. For this publication, we focus solely on the installation with the vibrodriver, which consists of the first 6 m.

3.1. Instrumentation setup

We utilize geophones, specifically the triaxial HL-6B-3C model from HGS Products, to convert ground vibrations (velocity) into analog voltage signals. Geophones comprise a coil suspended by delicate leaf springs around a permanent magnet. As the ground vibrates, the housing moves while the coil tends to remain stationary, inducing an electrical current proportional to the velocity of the vibration [25].

For the installation process, we utilized the ICE 24RF vibrator from International Construction Equipment (ICE). The essential technical specifications of this vibrator are detailed in Table 1. The manufacturer defines *dynamic weight* as the total mass subject to vertical oscillations (without any pile). Additionally, a type 200TU pile clamp with a weight of 1300 kg

was used. We established a geophone chain to capture the vibrations induced by pile driving. Each geophone was placed at a predetermined distance from the pile, as depicted in Fig. 1. The geophones were arranged in a straight line and levelled to ensure a horizontal orientation on the soil, facilitating precise vibration recording. We use the Sirius data acquisition system to collect and process the geophone measurements.

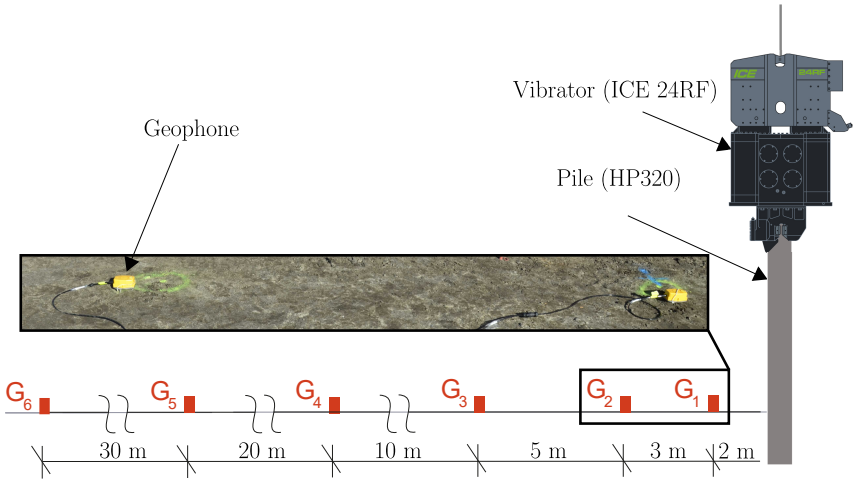

Figure 1: Arrangement of the geophones during the measurement campaign

Table 1: Technical data of the vibratory hammer without pile clamp

	Unit	ICE 24RF
Max. centrifugal force	kN	1400
Eccentric torque	kgm	0-24
Max. frequency	Hz	38.3
Max. tensile force	kN	400
Weight	kgf	3500
Dynamic weight	kgf	5960

4. Results and discussion

In the following section, we present the outcomes of applying standard and augmented DMD (AugDMD) to the dataset acquired during the measurement campaign.

The raw collected data from the geophones was initially sampled at 200 kHz to account for unforeseen effects caused by the soil heterogeneity and using the prebuilt anti-aliasing filter of the data acquisition hardware. Furthermore, more collected data could give us flexibility for the delay analysis. Fig. 2 presents a snapshot of the measurements captured by the first five geophones. Fig. 3 shows the frequencies present during the pile installation. During the measurements, the vibrator was operated at its maximum possible frequency. The component with the highest amplitude is located for all the geophones at approximately 39.18 Hz, which is close to the value corresponding to the maximum operating frequency of the vibrator mentioned in Table 1. After examining the present frequencies, shown in Fig. 3, we downsample the signal to 2kHz to simplify the subsequent analysis.

We see in Fig. 2 and Fig. 3 a rapid decrease in amplitude to the radial distance to the pile. Geophone 6 was deliberately excluded from the analysis due to its considerable distance from

the pile installation, primarily recording ambient noise rather than relevant vibration signals showing a negative signal-to-noise ratio (SNR).

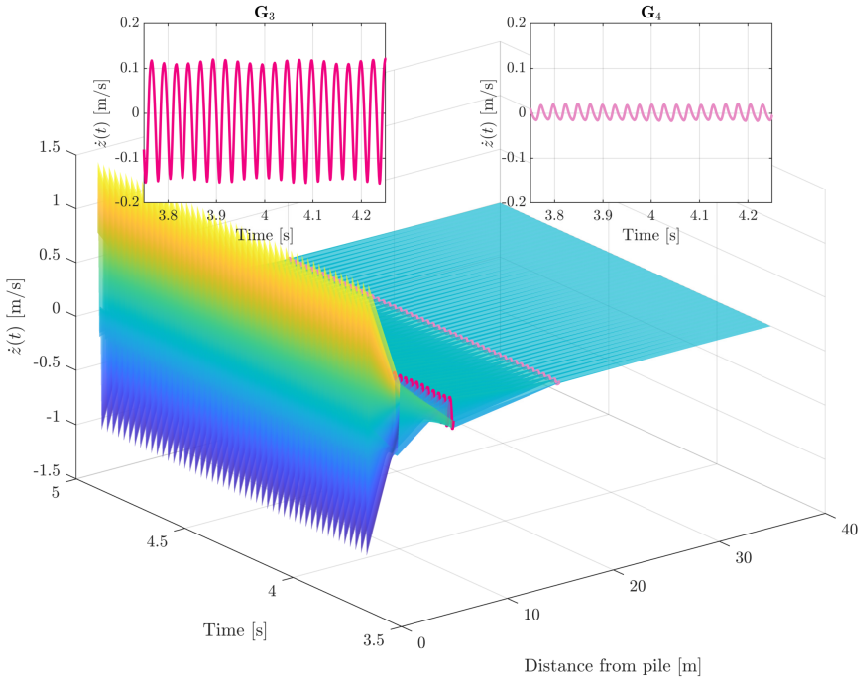

Figure 2: Vertical velocity $\dot{z}(t)$ with respect to the radial distance from the pile for the first five geophones. As an example, a zoom is shown for geophone 3 and 4

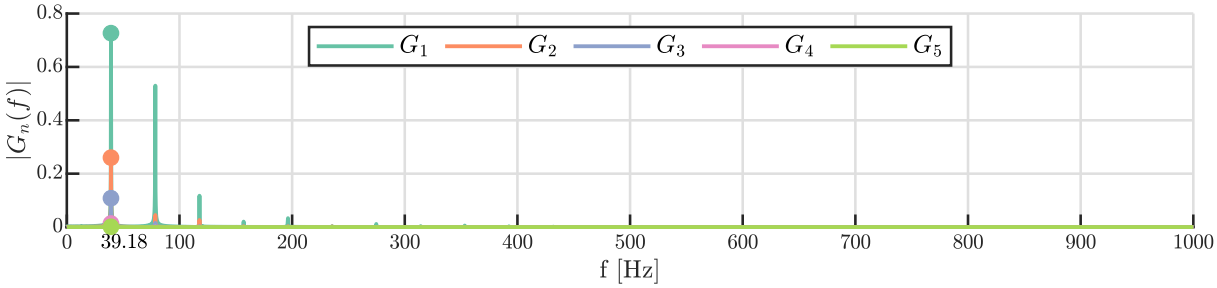

Figure 3: Results of applying the Fast Fourier Transform (FFT) algorithm to the signals recorded by the first five geophones

Even with the lowered sampling frequency, the dataset is extensive. Therefore, we opted to partition the collected data into two distinct extractions for a more manageable analysis. It's worth noting that similar outcomes were observed for the rest of the signal. The entire installation process of the third pile spans approximately 5 minutes. The specifics of these extractions are presented in Table 2. This partitioning strategy allows for a focused examination of the data, providing insights into the temporal evolution of soil vibrations during the vibrodriving process.

To measure the accuracy of both standard and augmented DMD as approximating and predicting tools, we employ the Normalized Root Mean Square Error (NRMSE) metric, as defined in Eq. 17.

Table 2: Time extractions of the third pile

Extraction	Time [s]	Penetration [m]
EA	1.55 - 2.00	0.9 - 1.0
EB	4.40 - 4.45	1.75 -2.0

$$\text{NRMSE} = \frac{\sqrt{\frac{1}{N}\sum_{i=1}^{N}|x_i - \hat{x}_i|^2}}{\max|\mathbf{x}_{G_j}| - \min|\mathbf{x}_{G_j}|} \tag{17}$$

Where x_i corresponds to the i entry of the time series of measured data of the j geophone $\mathbf{x}_{G_j}$ $(j = 1, 2, ...5)$ and $\hat{x}_i$ the resulting DMD-approximated or predicted data. N corresponds to the amount of samples considered in the error analysis.

In addition to the potential for controller design, the long-term objective of deploying the DMD for this application is the online in situ time-ahead predictions of the vibrations transmitted to the ground to serve as a warning mechanism and aid the operator in selecting feed parameters. However, this study concentrates on the proof of concept. Therefore, we simulate the online prediction by taking samples, deploying the DMD and augmented DMD algorithms, identifying the linear model, and using it to conduct time-ahead predictions of the vibrations. Then, we compare them with the actual measurements. This workflow would resemble one cycle of the theorized prediction tool. Accordingly, in the context of our analysis, *approximation* denotes the generation of the best-fitting linear dynamical system, in the least square sense, on the provided data. On the other hand, *time-ahead prediction* refers to applying the constructed linear system to foresee the system's future state in time.

4.1. Standard DMD

We begin with implementing the standard DMD algorithm for approximating and time-ahead predicting soil vibrations, as elaborated in Section 2.2. The outcomes of the approximation and time-ahead prediction of geophone data throughout the installation of the third pile are presented in Fig. 4 and Fig. 5.

Fig. 4 shows the outcomes for both approximation and time-ahead prediction for the first geophones data sequence, denoted as EA. The approximation is conducted considering the data collected during the initial 0.125 seconds (corresponding to 250 samples), followed by the time-ahead prediction of the subsequent 0.025 seconds (corresponding to 50 future samples). For the time-ahead prediction, the first 250 samples used for the approximation are employed to build the approximated linear dynamical system and then used for the time-ahead prediction following Eq. 4. The initiation of the prediction phase is indicated by $\mathbf{x}_{G_j}$ for $j = 1, 2, ..., 5$, corresponding to each geophone. Within this brief time window, the standard DMD approximation and time-ahead prediction results are relatively satisfactory, noticing the discrepancy for $\mathbf{G}_1$ due to its unique signal shape compared to the others.

Fig. 5 illustrates the outcomes for both approximation and time-ahead prediction for the second geophones data sequence, denoted as EB. Once again, the approximation encompasses the initial 0.125 seconds, and now we extend the time-ahead prediction for the subsequent 2.5 seconds or 5000 samples. We see that the predictive performance of the standard DMD sharply deteriorates over time. This degradation can be primarily attributed to identifying a dominant stable and purely real eigenvalue by the standard DMD, leading to a sharp decline in the amplitude of the solution over time for all geophones. These shortcomings become increasingly pronounced with an expanded time-ahead prediction timeframe. In both cases, the economy SVD is used without rank truncation.

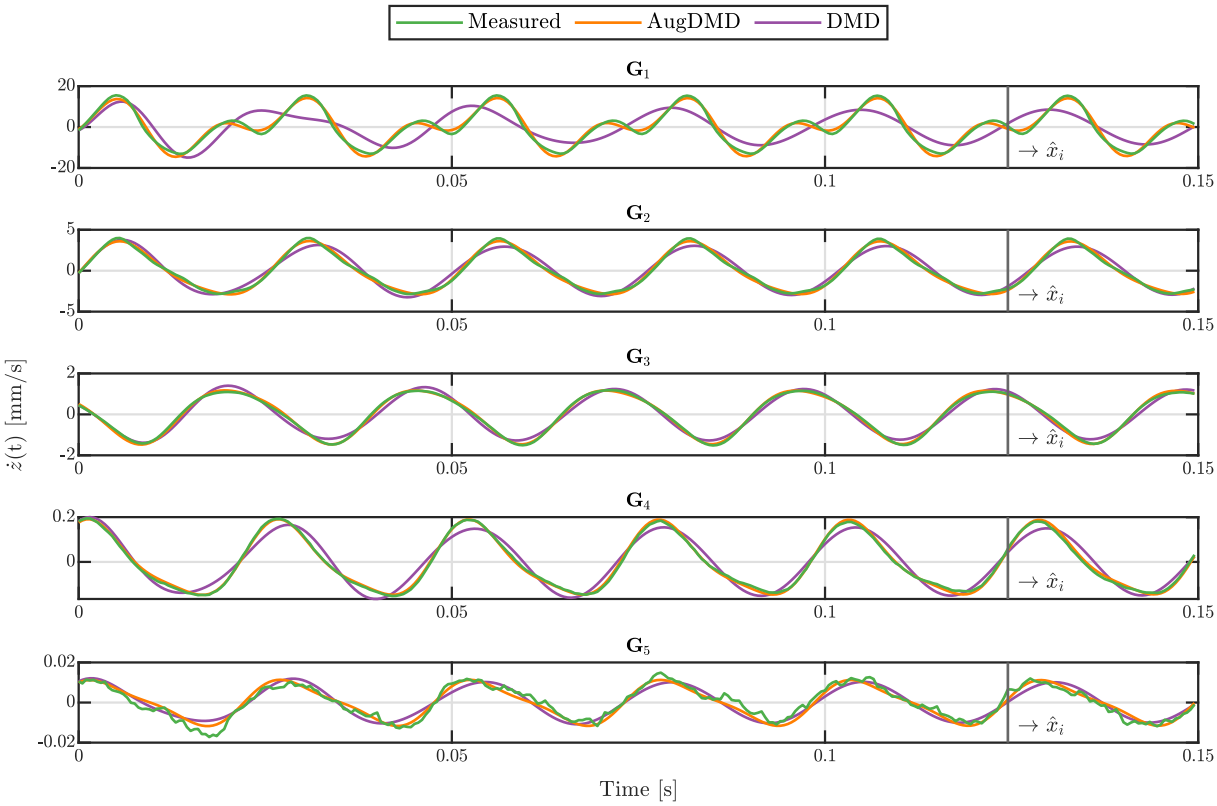

Figure 4: Approximation and prediction results of the standard and augmented DMD for EA

4.2. Augmented DMD

To improve the accuracy of the approximation and time-ahead prediction, we incorporate delayed coordinates, as described in Section 2.1. This time, we truncate the economy SVD to $r = 5$. The approximation and time-ahead prediction times remain the same as in the standard DMD case. Fig. 4 shows a comparable agreement with standard DMD, highlighting AugDMD's slight outperformance for this abbreviated time window. Notably, AugDMD captures the shape of $\mathbf{G}_1$ more effectively. Furthermore, for the longer time window shown in Fig. 5, a considerable improvement in accuracy is evident compared to standard DMD. We notice, however, that for $\mathbf{G}_1$, the AugDMD result shows a slight amplitude increase with time.

For the AugDMD, we select 50 delay coordinates, corresponding to considering an extra entire period of the signal captured by the geophones, equivalent to approximately 0.025 seconds. To corroborate the advantage of this selection of delay coordinates, we deployed the AugDMD algorithm, varying the number of delayed coordinates from 1 to 101 in steps of 10, and we calculated the NRMSE as per Eq. 17 to the actual signal. The results, depicted in Fig. 6, reassure our choice of delay coordinates, demonstrating a sharp decrease in error at around 50 delay coordinates in both EA and EB. This systematic approach ensures the selection of an adequate number of delay coordinates, enhancing the accuracy of AugDMD.

We further assess the effectiveness of the AugDMD for time-ahead predictions, maintaining the approximation time of 0.125 and expanding the prediction time. We then calculate the NRMSE between the measurement data and the time-ahead prediction, as illustrated in Fig. 7, which reveals an increasing error with longer prediction times. This trend originates from the dynamic changes in soil vibrations during the vibrodriving process, influenced by evolving local soil conditions.

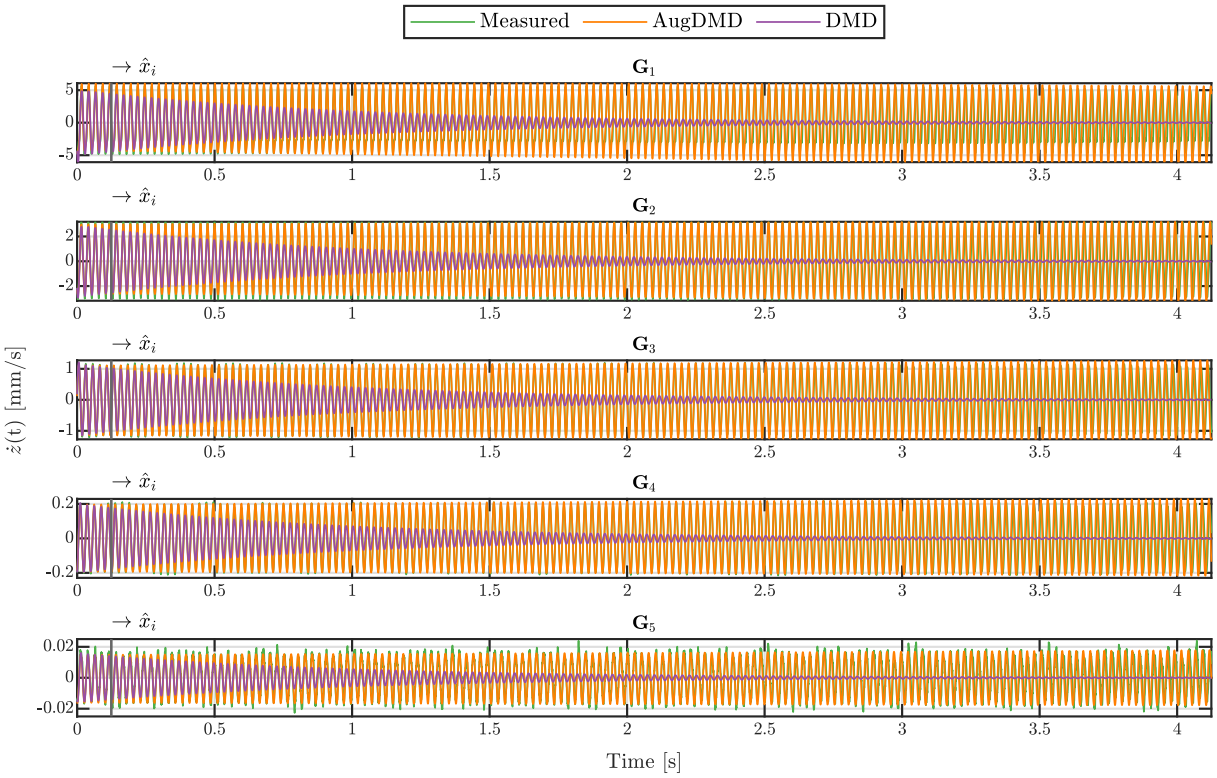

Figure 5: Approximation and prediction results of the standard and augmented DMD for EB

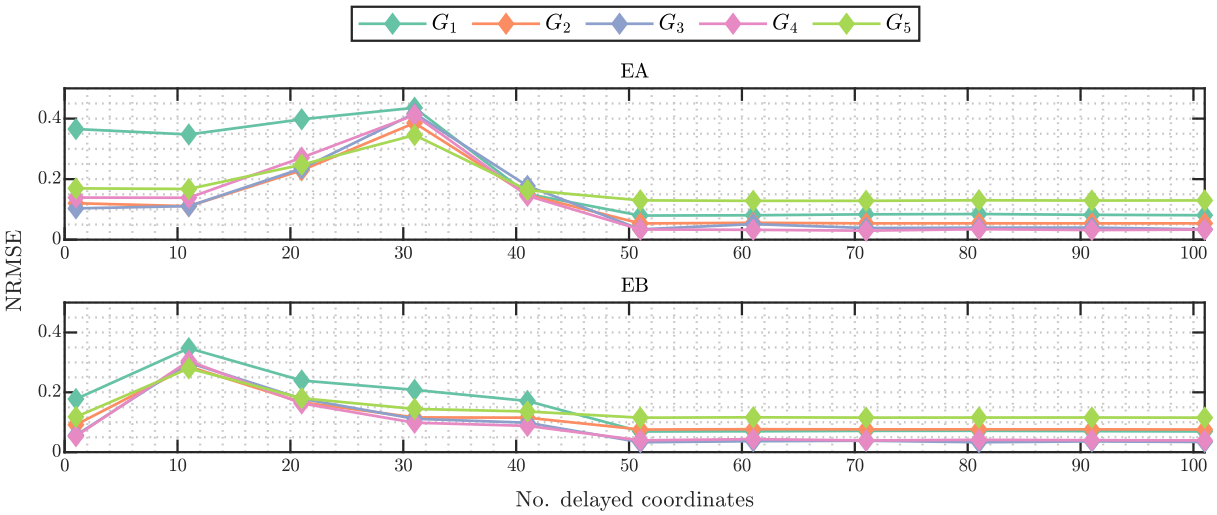

Figure 6: NRMSE for EA and EB for an increase in the number of delayed coordinates using the AugDMD

The growing NRMSE underscores the necessity of online deployment for AugDMD, where data is continually updated. Despite this, the results demonstrate the clear potential of AugDMD as a reliable prediction tool for time-ahead prediction of soil vibrations. A valid prediction can be achieved by consistently updating the time window for AugDMD calculations while keeping the time-ahead prediction short. This technique offers a practical and purely data-driven solution for field applications.

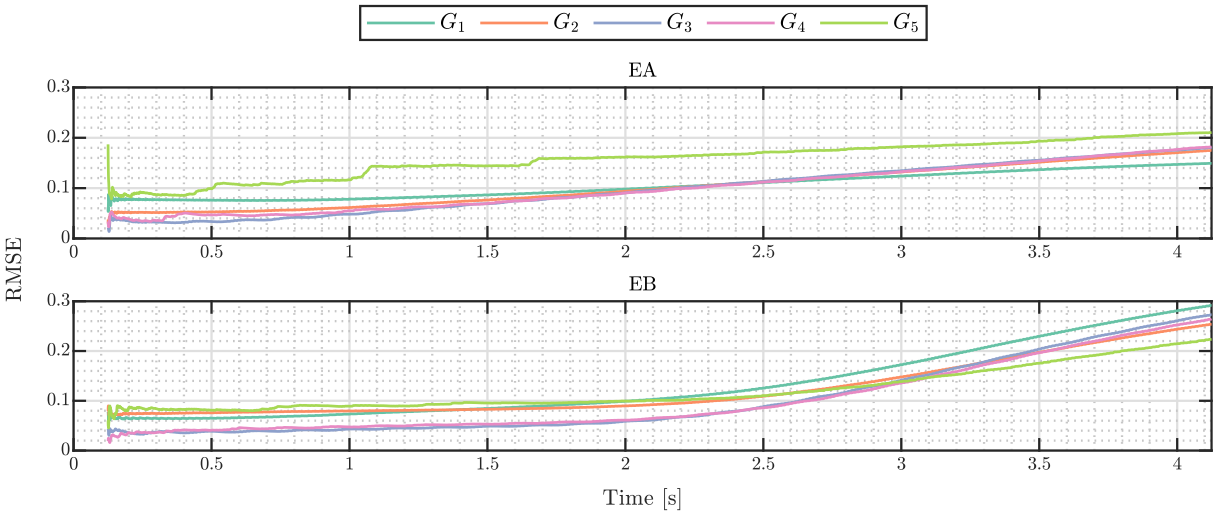

Figure 7: NRMSE for time-ahead predictions of EA and EB using the AugDMD

5. Conclusion and further research

This study introduces a purely data-driven methodology utilizing standard and augmented Dynamic Mode Decomposition (DMD) to address the challenge of modeling and predicting soil vibrations during the vibrodriving process. The outcomes demonstrate the potential of this data-driven technique in accurately approximating soil vibrations and predicting and monitoring the system's future behavior. The methodology shows promise as an online prediction tool, with augmented DMD proving more efficient. An extension of this work would involve using DMD with control (DMDc), where including control parameters, such as the rotational frequency of eccentric weights or torque, could significantly boost prediction accuracy. This extension would allow the development of a warning system, enabling operators to receive timely alerts if newly chosen feed parameters approach potentially hazardous values based on DMDc predictions. Integrating control parameters into the DMD framework paves the way for the methodology to evolve into a robust real-time monitoring and decision-support tool.

The envisioned process begins with preparing the pile and geophones, as described in this work. In addition, sensors should be installed to measure the torque and rotational frequencies of the eccentric masses. A real-time system, such as a Beckhoff PLC with TwinCAT 3 runtime environment, is then set up to collect sensor data and calculate predictions. The vibrodriving process commences with the use of empirically determined feed parameters. Simultaneously, the real-time system collects time-synchronized data from the torque and geophones. After collecting sufficient samples, the DMDc machinery creates a local linear model that approximates the vibrator-pile-soil dynamics solely based on the collected data. The system continuously updates the linear model for a moving time window, running in parallel during the vibrodriving process. If significant prediction errors occur, adjustments may be made to the parameters, necessitating further study for online parameter tuning. When the operator modifies the frequency (and torque) of the vibrator, a time-ahead prediction of expected vibrations in the geophones is calculated. If the predicted vibrations exceed a pre-established limit, a warning is issued to prevent potential damage to neighboring structures. In conclusion, this study demonstrates the effectiveness of DMD in soil dynamics and lays the groundwork for future advancements. Using a purely data-driven technique such as DMD reduces the required a priori knowledge of soil conditions and minimizes the need for laboratory tests.

Acknowledgments
Acknowledgments This research is funded by the German Federation of Industrial Research Associations – AiF, within the framework of the "SmartVIB" project.

References
[1] Chrisopoulos S and Triantafyllidis T 2019 *Bautechnik* **96** 176–194
[2] Ramshaw C and Selby A 2003 *Computational Modelling in Hydraulic and Coastal Engineering* ed Bull J (Spon Press) chap 5, pp 132–167
[3] Rodger A and Littlejohn 1980 *Géotechnique* **30** 269–293
[4] Meshcheriakov G and Andryushchenko A 2023 *Proc of the 40th International Symposium on Automation and Robotics in Construction (Chennai)* pp 172–179
[5] Heikkilä R, Kivimäki T and Puolitaival K 2010 *Proc of the 27th International Symposium on Automation and Robotics in Construction (Bratislava)* pp 73–80
[6] Massarsch K, Fellenius B and Bodare A 2017 *Geotechnik* **40** 126–141
[7] Wiss J 1967 *Highway Research Record* **155** 14–20
[8] Bornitz G 1931 *Über die Ausbreitung der von Großkolbenmaschinen erzeugten Bodenschwingungen in die Tiefe* (Heidelberg: Springer Berlin)
[9] Jongmans D 1996 *Engineering Geology* **42** 25–36
[10] Attewell P and Selby A 1992 *Geotechnical and Geological Engineering* **10** 41–59
[11] Sun Z, Yu C, Li C, Liu R, Li Q and Su C 2023 *Buildings* **13** 1884
[12] Henke S and Grabe J 2009 *Proc. Int. Conf. on Soil Mechanics and Geotechnical Engineering (Alexandria)* vol 1,2,3,4 (IOS Press) pp 1321–1324
[13] Henke S 2010 *International Journal for Numerical and Analytical Methods in Geomechanics* **34** 1191–1210
[14] Grabe J and Mahutka K 2005 *Bautechnik* **82.9** 632–640
[15] Reusch D 2000 *Proc. of the 17th International Symposium on Automation and Robotics in Construction (Taipei)* pp 1–6
[16] Musgrave D, Bingham C, Stone D and Howe D 2000 *IEE Proc Electr Power Appl* **147** 345–352
[17] Bingham C, Stone D, Schofield N, Howe D and Peel D 2000 *IEEE Transactions on Industrial Electronics* **47** 623–631
[18] An Z, Zhang N and Jia Y 2023 *J. Phys.: Conf. Ser.* **2174** 012076
[19] Schmid P 2010 *Journal of Fluid Mechanics* **656** 5–28
[20] Kutz J, Brunton S, Brunton B and Proctor J 2016 *Dynamic Mode Decomposition: Data-Driven Modeling of Complex Systems* (Philadelphia: Society of Industrial and Applied Mathematics)
[21] Brunton S and Kutz J 2022 *Data-driven science and engineering: machine learning, dynamical systems, and control* (Cambridge: Cambridge University Press)
[22] Strang G 2014 *Linear Algebra and Its Applications* (Belmont: Thomson, Brooks/Cole)
[23] Strang G 2019 *Linear Algebra and Learning from Data* (Wellesley: Wellesley-Cambridge Press)
[24] Alkateeb D, Künzel A, Dogan A and Grabe J 2023 *Tagungsband zum Pfahl-Symposium 2023 in Braunschweig* (*Mitteilung des Instituts für Geomechanik und Geotechnik der Technischen Universität Braunschweig* vol 1) pp 351–368
[25] Iskander M 2018 *Underground Sensing* (Elsevier) pp 141–202